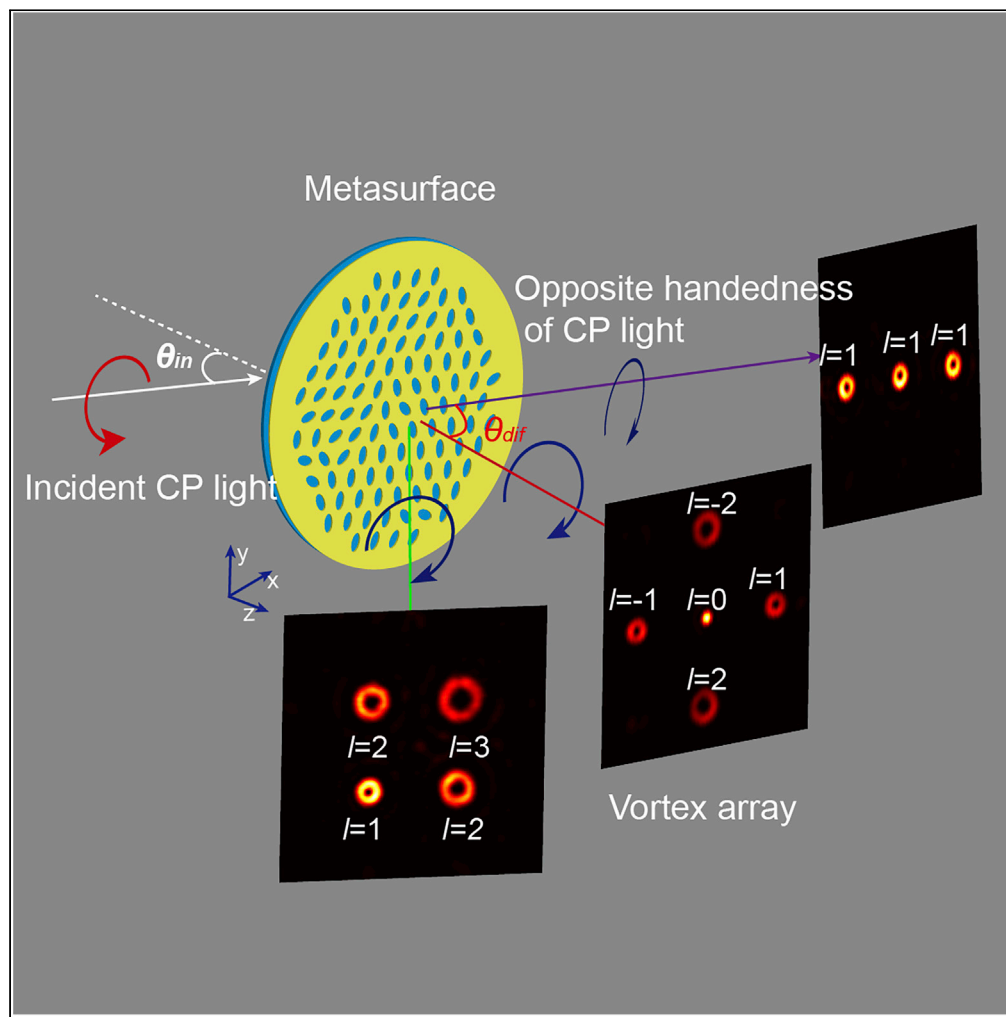


Article

Angular-multiplexed multichannel optical vortex arrays generators based on geometric metasurface



Jinjin Jin, Xiong Li,
Mingbo Pu, ...,
Mingfeng Xu,
Zuojun Zhang,
Xiangang Luo

lxg@ioe.ac.cn

HIGHLIGHTS

Ultra-thin angular-multiplexed multichannel vortex array generators are demonstrated

Geometric phase is employed to realize the desired phase profiles

Generation of various multichannel vortex arrays and recombination of vortex array

Jin et al., iScience 24, 102107
February 19, 2021 © 2021 The Authors.
<https://doi.org/10.1016/j.isci.2021.102107>

Article

Angular-multiplexed multichannel optical vortex arrays generators based on geometric metasurface

Jinjin Jin,¹ Xiong Li,^{1,2} Mingbo Pu,^{1,2} Yinghui Guo,^{1,2} Ping Gao,¹ Mingfeng Xu,^{1,3} Zuojun Zhang,¹ and Xiangang Luo^{1,2,4,*}

SUMMARY

Recently, metasurface-based multichannel optical vortex arrays have attracted considerable interests due to its promising applications in high-dimensional information storage and high-secure information encryption. In addition to the well-known wavelength and polarization multiplexing technologies, the diffraction angle of light is an alternative typical physical dimension for multichannel optical vortex arrays. In this paper, based on angular multiplexing, we propose and demonstrate multichannel optical vortex arrays by using ultrathin geometric metasurface. For a circularly polarized incident light, the desired optical vortex arrays are successfully constructed in different diffraction regions. Moreover, the diffraction angle of the optical vortex array can be regulated by changing the illumination angle of incident light. Capitalizing on this advantage, the angular-multiplexed recombination of optical vortex array is further investigated. The combination of the diffraction angle of light and optical vortex array may have significant potential in applications of optical display, free-space optical communication, and optical manipulation.

INTRODUCTION

In 1992, Allen et al. recognized that lights in paraxial regime with spiral phase front manifesting as an azimuthal phase term $\exp(i\ell\phi)$ would carry an orbital angular momentum (OAM) of ℓh per photon (Allen et al., 1992), where ϕ is the azimuthal angle and ℓ is topological charge. The striking optical properties of vortex light (OAM light) have attracted great attentions in many areas, such as super-resolution imaging (Tamburini et al., 2006), optical micromanipulation (Dholakia et al., 2008), and detection of rotating objects (Lavery et al., 2013). Especially, the unbounded orthogonal modes of ℓ have provided a new degree of freedom for information encoding to improve the capacity and security of the free-space optical communication systems (Gibson et al., 2004). In order to realize multi-channel communication by vortex beams, vortex light array has been proposed and investigated. Several methods have been put forward to generate the optical vortex array, such as phase diffractive optical elements (Khonina et al., 2001), spatial light modulators (Gibson et al., 2004), and Damman vortex grating (Lei et al., 2015). However, the bulky size of such elements cannot fulfill the requirement of miniaturization, integration, and multifunction of the modern optical system.

Recently, metasurface (Huang et al., 2012; Ni et al., 2013a; Pu et al., 2015a, 2015b; Yu et al., 2011), a two-dimensional artificial metamaterial, has been taken as a candidate of conventional bulky optical element. One of the important advantages of the metasurface is its great capability of amplitude, polarization, wavelength, and phase manipulation of electromagnetic waves by properly adjusting the geometry and the orientation of the subwavelength scale structures at the ultrathin interface. Flat lenses (Aieta et al., 2012; Yu and Capasso, 2014), meta-holograms (Guo et al., 2019; Huang et al., 2013; Li et al., 2016; Ni et al., 2013b; Zhang et al., 2017), beam splitters (Li et al., 2015; Lin et al., 2013), and multifunctional devices (Chen et al., 2020; Ma et al., 2019; Wen et al., 2016; Zhang et al., 2020a) were realized in an ultrathin and compact way. More recently, metasurface-based optical vortex arrays have been studied (Jin et al., 2017; Liu et al., 2016; Zhang et al., 2020b). To further improve the capacity and security of device, the multichannel vortex arrays based on metasurface were also extensively investigated (Huang et al., 2017; Jiang et al., 2018; Jin et al., 2018; Liu et al., 2016; Ren et al., 2016, 2019). For instance, Huang et al. investigated the generation of three-dimensional volumetric vortex arrays based on ultrathin geometric metasurface

¹State Key Laboratory of Optical Technologies on Nano-Fabrication and Micro-Engineering, Institute of Optics and Electronics, Chinese Academy of Sciences, P.O. Box 350, Chengdu 610209, China

²School of Optoelectronics, University of Chinese Academy of Sciences, Beijing 100049, China

³Division of Frontier Science and Technology, Institute of Optics and Electronics, Chinese Academy of Sciences, Chengdu 610209, China

⁴Lead contact

*Correspondence: lxg@ioe.ac.cn

<https://doi.org/10.1016/j.isci.2021.102107>



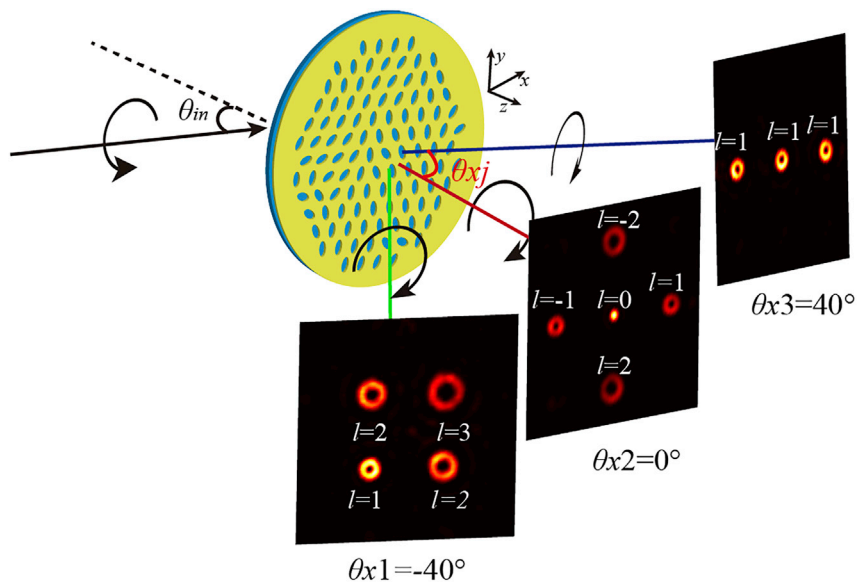


Figure 1. Schematic of multichannel optical vortex arrays based on ultrathin geometric metasurface

The lights with different colors represent different diffraction angles. θ_{in} represents the angle of incidence; θ_{xj} ($j = 1, 2, 3 \dots$) represents the diffraction angle.

(Huang et al., 2017). Along the longitudinal propagation direction, a sequence of coaxial two-dimensional vortex arrays was reconstructed through the metasurface, leading to space multiplexing. On the other hand, the wavelength selectivity of metasurface provides another possibility for the generation of multichannel vortex arrays. Jin et al. reported a wavelength-multiplexed metasurface that could produce different three-dimensional optical vortex arrays by changing the wavelength of the incident light (2018; Jin et al.). In fact, polarization and OAM of light can also be regarded as the multiplexing method to modulate vortex arrays. Jiang et al. demonstrated a spin-dependent two-channel vortex beam generator based on metasurface (Jiang et al., 2018). Ren et al. achieved an OAM-conserving meta-hologram, wherein various holographic images composed by optical vortex arrays appeared when light with corresponding OAM illuminates the designed metasurface (Ren et al., 2019). The flexible electromagnetic control of metasurface has provided versatile multiplexing methods for producing the multichannel optical vortex arrays. In addition to the above proposed multiplexing methods, the diffraction angle of light can also be used to modulate vortex arrays effectively. However, to the best of our knowledge, there have been no reports on the generation of multichannel optical vortex arrays with angular-multiplexed metasurfaces.

In this paper, based on the angular multiplexing, the multichannel optical vortex arrays generators are investigated and experimentally demonstrated by using the ultrathin geometric metasurface. The metasurface consists of an array of elliptical nanoholes with spatially varying orientation. When a circularly polarized light is incident on the nanoholes, it generates the desired phase profile for the excited opposite handedness component. By a proper design of metasurface, various vortex arrays diffract at different angles on the transmission side. The pattern and topological charge of the vortex array in each channel can be independently determined. Particularly, the diffraction angle of the vortex array is related to the illumination angle, which means that one can recombine a new vortex array by regulating the illumination angle of incident light, leading to a remarkable enhancement of the optical information security. The multiplexing approach proposed in our work provides an effective way to increase the storage capacity and encryption security of subwavelength optical devices.

RESULTS AND DISCUSSIONS

The angular-multiplexed multichannel vortex arrays mean that a sequence of vortex arrays with various topological charges diffracted in the azimuthal direction, as depicted in Figure 1. The implementation of the function depends on the ultrathin geometric metasurface. The metasurface used in our design is composed of elliptical nanohole arrays in a thin metallic film with desired orientation angle φ with respect to the positive x direction. Under the illumination of circularly polarized light, the elliptical nanohole array

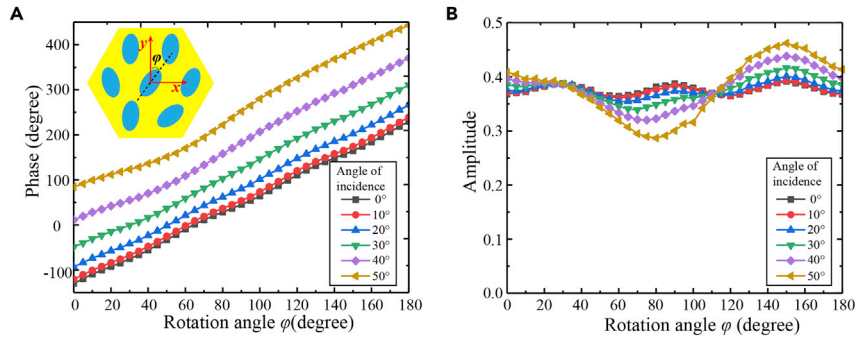


Figure 2. Phase and amplitude profiles of the unit cell

(A) The phase change as a function of the orientation angle of the unit cell with different illumination angles at a wavelength of 632.8 nm.

(B) The amplitude shift as a function of rotation angle of the unit cell with different illumination angles. The period of the unit cell is 250 nm. The long axis and short axis length of the nanohole in the simulation are 200 nm and 110 nm, respectively. The thickness of the gold film is 70 nm. The lines with different colors and symbols represent the simulation results at different incident angles.

provides the desired phase profile to the scattered light of the opposite handedness. The relationship between the phase shift and orientation angle of elliptical nanoholes is $\Phi = \pm 2\varphi$, namely Pancharatnam-Berry or geometric phase shift, where the signs “+/-” correspond to the left-handed circular polarization (LCP)/right-handed circular polarization (RCP) incident light. By controlling the orientation angle of elliptical nanoholes from 0 to π , phase shift covering 0 to 2π can be achieved. In our design, each elliptical nanohole is placed at the center of the hexagonal lattice with a lattice constant of 250 nm. The subwavelength size of the unit cell guarantees that the light emitted by the metasurface would not diffract to the higher diffraction orders apart from the zeroth order. The phase profiles of elliptical nanoholes are simulated by the commercial electromagnetic simulation software of CST Microwave Studio. Figure 2A illustrates the phase profile as a function of the orientation angle of the unit cell at a wavelength of 632.8 nm with LCP incidence. Taking the off-axis illumination into consideration, the phase shifts of the unit cell at the different illumination angles are investigated. It can be seen that the phase change covers full 0 to 2π range when the illumination angle of circularly polarized light changes from 0° to 50°. In general, with the change of rotation angle, the generated amplitude of the scattered opposite helicity light maintains nearly consistent because of the unifying size and shape of the elliptical nanohole, as depicted in Figure 2B. The amplitude profiles under the circumstance of different illumination angles are also simulated. It is shown that the nearly equal transmission amplitude is achieved when the angle of incidence changes from 0° to 50°. The conversion efficiency of the elliptical nanoholes can also be obtained in the simulation, which is about 31%. By elaborately encoding the orientation angle and the arrangement of elliptical nanoholes, the desired function can be achieved.

To achieve angular multiplexing, we employ the principle of superimposition of holograms (Pu et al., 2015b), which can incorporate the information from all angles in a 2D plane. Various vortex arrays with different additional phase shifts are linearly superimposed. The integrated complex field can be expressed as follows:

$$E_{\text{tot}}(x, y, \lambda, l, k_x, k_y) = \sum_{j=1}^N E_j(x', y', \lambda, l, \lambda) e^{-i(k_{xj}x + k_{yj}y)}. \quad (\text{Equation 1})$$

where E_{tot} is the complex amplitude of the synthetic multichannel vortex arrays, N represents the total number of vortex array, $k_{xj} = k_0 \sin \theta_{xj}$ and $k_{yj} = k_0 \sin \theta_{yj}$ are the wave vectors, which determine the diffraction angle of single channel vortex array in the x and y direction, respectively, θ_{xj} and θ_{yj} are the diffraction angles relative to the x and y axis, respectively. E_j is the individual complex field of a vortex array without any inclination, which can be written as follows:

$$E_j(x', y', \lambda, l, \lambda) = \sum_m \sum_n A_{mn} e^{ilmn} e^{-i \left(\frac{2\pi}{\lambda} \left(\sqrt{(x' - x'_m)^2 + (y' - y'_n)^2 + f^2} - f \right) \right)} \quad (\text{Equation 2})$$

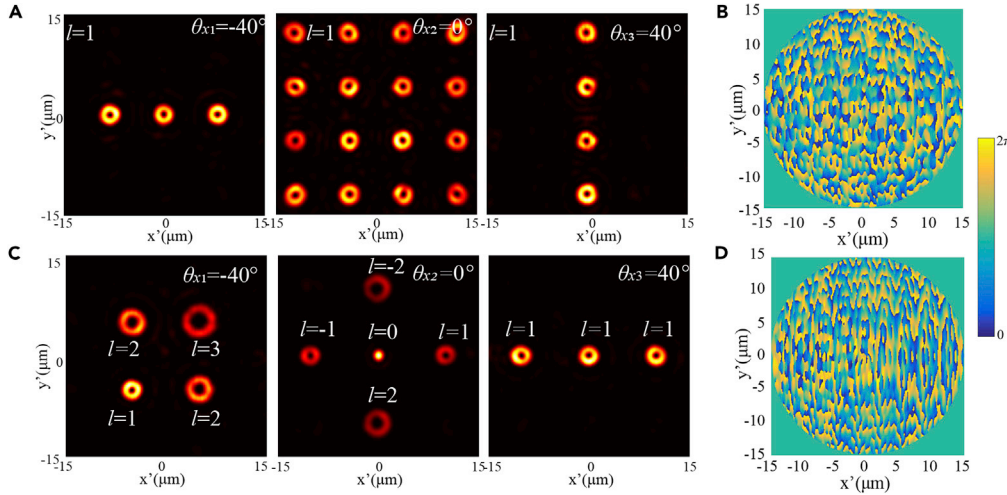


Figure 3. Intensity and phase profiles of the multichannel vortex arrays generator

(A) Simulated light intensity distribution of the first multichannel vortex arrays generator. The diffraction angle of the left, middle, and right images $\theta_{x1} = -40^\circ$, $\theta_{x2} = 0^\circ$, and $\theta_{x3} = 40^\circ$, respectively. The topological charge of three channels vortex array is uniformly defined as $l = 1$. The focal length of vortex array is set as $f = 50 \mu\text{m}$.

(B) The phase profile of the first multichannel vortex arrays generator.

(C) The theoretical light intensity distribution of the second multichannel vortex arrays generator.

(D) The phase profile of the second multichannel vortex arrays generator.

where x' and y' are the local coordinates, and m and n represent the diffraction orders in the x' and y' directions, respectively, for each single vortex beam in the vortex array. A_{mn} is the amplitude distribution of single vortex light with a topological charge of l_{mn} . In order to capture the vortex array at a certain plane, the phase profile of $\frac{2\pi}{\lambda} \left(\sqrt{(x' - x'_m)^2 + (y' - y'_n)^2 + f^2} - f \right)$ is superimposed onto the vortex beam, where f is the focal length of transmitted light, and (x'_m, y'_n) represents the focus location of a vortex beam at (m, n) diffraction order. According to the Equations (1) and (2), the diffraction angle and the topological charge of the vortex array can be determined independently.

The light field acquired from Equation (1) can be performed by phase-only modulated metasurface. The phase profile imparted to the metasurface can be written as follows:

$$\Phi(x, y, \lambda, l, k_x, k_y) = \arg(E_{\text{tot}}(x, y, \lambda, l, k_x, k_y)). \quad (\text{Equation 3})$$

More remarkably, the diffraction angle of vortex arrays is also related to the angle of incidence, that is, we can regulate the vortex array to the desired diffraction angle by changing the illumination angle of the incident light. Meanwhile, this process allows us to recombine the arrangement form of the vortex array.

To validate the capability of the angular multiplexing, several multichannel vortex arrays generators based on geometric metasurfaces are designed and fabricated. We first perform two angular-multiplexed multichannel vortex arrays generators operating at a wavelength of 632.8 nm. Here, for experimental simplicity and sufficient separation between the two vortex arrays, the channel number of the two samples in design is uniformly set as $N = 3$, and the diffraction angle of the three light arrays is set as $\theta_{x1} = -40^\circ, \theta_{y1} = 0^\circ, \theta_{x2} = 0^\circ, \theta_{y2} = 0^\circ$, and $\theta_{x3} = 40^\circ, \theta_{y3} = 0^\circ$, respectively. In principle, the diffraction angle and number of vortex array are unconstrained. However, considering the size of vortex array, the finite angle range of free space, and the light cross talk, the diffraction angle and channel number of vortex array are limited in the actual design process (detailed discussion shown in Section S1, Supplementary Information). In the numerical simulations, the reconstructed light intensity profile for the first multichannel vortex arrays generator is shown in Figure 3A, where the vortex arrays diffracted in three channels are designed as 1×3 , 4×4 , and 4×1 vortex array, respectively. The topological charge of all the vortex beams for this generator is uniformly defined as $l = 1$. For the second multichannel vortex array generator, the light intensity distributions of the vortex arrays at different channels are shown in Figure 3C, where the form of three vortex arrays is defined as 2×2 vortex array, rhombus vortex array, and 1×3 vortex array, respectively. In order to illustrate the

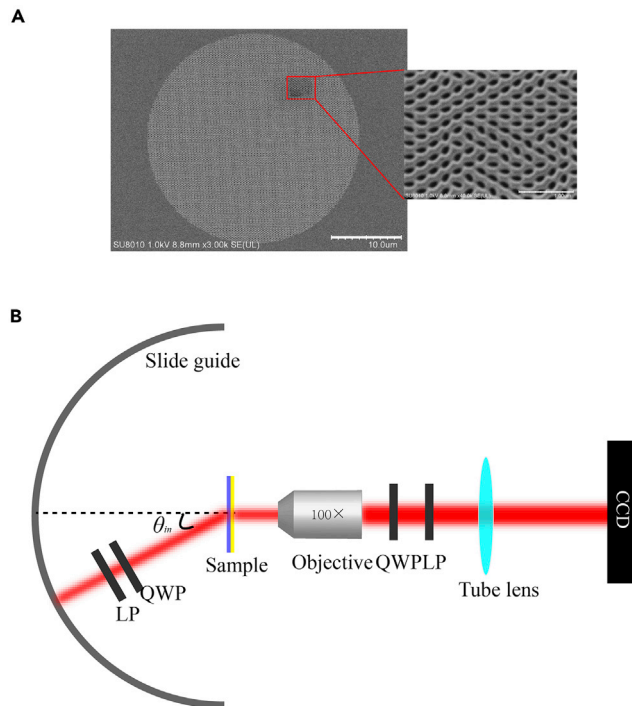


Figure 4. SEM image and experimental setup of the fabricated metasurface

(A) Schematic of SEM image of the first angular-multiplexed multichannel vortex arrays generator. The major axis and minor axis of the elliptical nanohole are 200 nm and 110 nm, respectively.

(B) Schematic of experimental setup.

flexibility of the design, the topological charge in the vortex array produced by the second multichannel vortex arrays generator is spatially variant. Then, we resort to Equation (1) to superimpose the lights diffracted at different angles. The corresponding phase profiles obtained by Equation (2) are illustrated in Figures 3B and 3D. Note that the center of the focus plane of vortex array is placed at a distance of 50 μm from the metasurface center.

A scanning electron microscopy (SEM) image of the fabricated metasurface is displayed in Figure 4A. The elliptical nanoholes are milled by using the focused ion beam in a 70-nm-thick gold film on the glass substrate. The effective area of each metasurface is a circle with a radius of 15 μm. Since the scattered lights are diffracted into different angles, it is difficult to capture all vortex arrays on the same plane. As mentioned above, the diffraction angle of the light array is related to the illumination angle of incident light, and the change of the illumination angle will alter the direction of emitted light without affecting the reconstruction of the vortex beam. Therefore, by changing the illumination angle of incident light during the test, three diffraction vortex arrays will be captured separately at the desired diffraction angle. To simplify the measurement, we make the detection plane coaxial with the metasurface to capture the transmission light with 0° diffraction angle, as depicted in Figure 4B.

Figure 5A presents the experimental results of the first multichannel vortex arrays generator. The switching among different vortex array channels is achieved by tuning the illumination angle of the incident light. When the illumination angle is set as $\theta_{in} = 40^\circ$, the 1×3 vortex array appears at the 0° diffraction angle at the position of $z = 50 \mu\text{m}$ (left image in Figure 5A). The light array changes to a 4×4 vortex array as the light is normally incident on the metasurface (middle image in Figure 5A). A 4×1 vortex array is reconstructed when the illumination angle of light is adjusted as $\theta_{in} = -40^\circ$ (right image in Figure 5A). The measured results of the second multichannel vortex arrays generator are depicted in Figure 5B. When the illumination angle of light is set as $\theta_{in} = 40^\circ$, $\theta_{in} = 0^\circ$, and $\theta_{in} = -40^\circ$, respectively, a 2×2 vortex array (left image in Figure 5B), rhombus vortex array (middle image in Figure 5B), and 1×3 vortex array (right image in Figure 5B) successively appear in the imaging area. The topological charge in each vortex array is

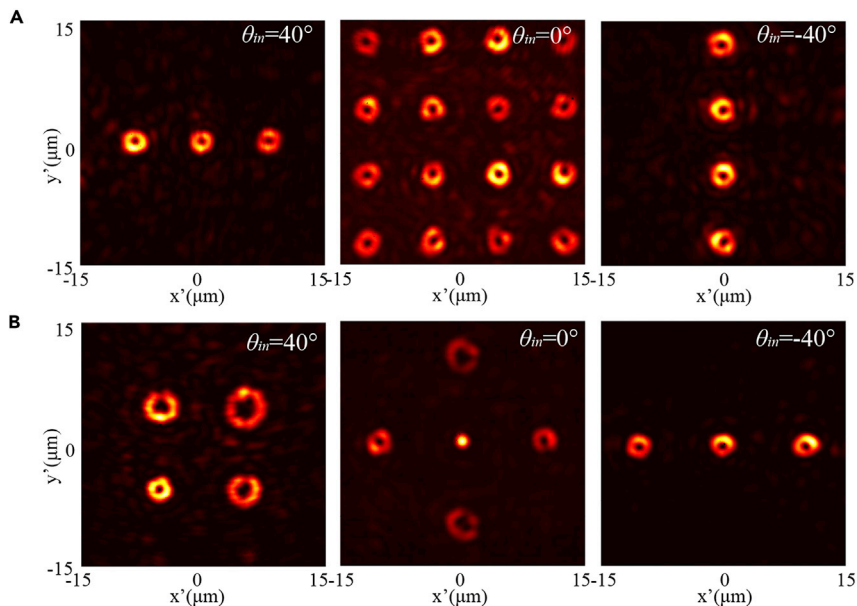


Figure 5. Schematic of measured results of the two fabricated generators

(A) Measured results of the first multichannel vortex arrays generator for different illumination angles.

(B) Measured results of the second multichannel vortex arrays generator for different illumination angles.

variant, which agrees well with the theoretical results. The maximum field angle of the generated vortex array for the two generators is about 31° , which is less than the diffraction angle difference of the two adjacent vortex arrays (the difference is 40°). Therefore, there is no cross talk between the reconstructed vortex arrays. Although the generators are designed at the wavelength of 632.8 nm, it also can work at other wavelengths owing to the dispersion-less phase property of the geometric metasurface. We verified the broadband property of the designed generators by measuring the diffraction intensity profiles at different wavelengths from 532 nm to 670 nm, as shown in [Figures S3 and S4 \(Supplementary Information\)](#). Subsequently, the conversion efficiency defined as the ratio of the vortex arrays beam to the overall transmitted power is measured, which is about 18% at wavelength of 632.8 nm in the experiment. Compared with the numerical result, the reduction may originate from the light reflection, experimental errors, and imperfect fabrication. The conversion efficiency can be further improved by using the dielectric metasurface ([Zhang et al., 2020b](#)) or changing to the multilayer reflective type metasurface ([Zheng et al., 2015](#)).

The experiment results of the fabricated multichannel vortex arrays generators indicate that the diffraction angle of multichannel vortex arrays can be manipulated by changing the illumination angle of incident light, which means that one can recombine the arrangement form of the diffracted vortex array by regulating the illumination angle. We further investigate the recombination of the vortex array by employing angular multiplexing based on geometric metasurface. As depicted in [Figure 6A](#), the desired vortex array is reconstructed at a certain diffraction angle only when two beams with different illumination angles are incident on the metasurface simultaneously. The purpose of the design is to generate a number of “8” consisting of vortex beams (right image in [Figure 6B](#)) with topological charge of 1 along the 0° diffraction angle. The implementation of this type of vortex array requires the combination of two kinds of vortex arrays, namely, one is the letter “E” (left image in [Figure 6B](#)) and the other is the number “1” (middle image in [Figure 6B](#)). The initial diffraction angle of two kinds of vortex arrays is $\theta_{x1} = -40^\circ$ and $\theta_{x2} = 40^\circ$, respectively. Thus, when the circularly polarized light is normally incident on the device, there is no vortex array reconstructed at the 0° diffraction angle. While when the incident angle of light is only set as $\theta_{in} = 40^\circ$ or $\theta_{in} = -40^\circ$, the letter “E” or number “1” appears alone at the 0° diffraction angle. The complete vortex array can be reconstructed at 0° diffraction angle under the condition that two incident light beams with different illumination angles irradiate the sample at the same time. The phase profile of the generator is shown in [Figure 6C](#). The performance of the fabricated metasurface is measured by modifying the experimental setup shown in [Figure 4B](#). In order to realize the simultaneous illumination of two incident light beams,

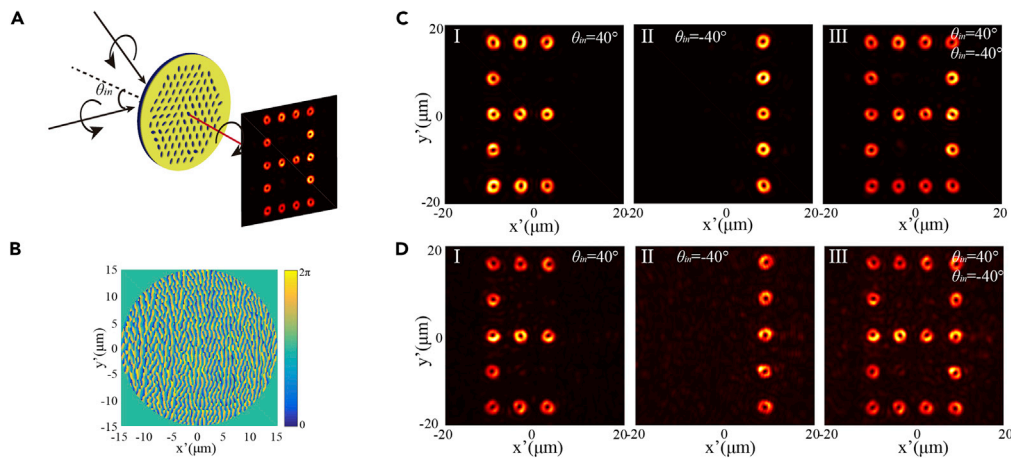


Figure 6. Schematic of the recombination of vortex array and the characterization results

- (A) Schematic of angular-multiplexed recombination of vortex array.
 (B) Theoretical results of vortex array recombination generator. The light intensity images at left, middle, and right are the letter "E" diffracted to an angle of -40° , the number "1" diffracted to an angle of 40° , and recombined complete vortex array, respectively. The topological charge of each vortex beam is 1.
 (C) The phase profile of vortex array recombination generator.
 (D) The corresponding experimental results.

a beam splitter is adapted to divide the He-Ne laser into two incident light beams. The detective system is coaxial with the fabricated metasurface to receive the transmission light propagated at the 0° diffraction angle. The illumination angle of two incident lights is adjusted to 40° and -40° , respectively. When the illuminate light at 40° is blocked, the image of number "1" is detected at the plane $50\ \mu\text{m}$ away from the metasurface, as depicted in middle image in Figure 6D. While the detected vortex array profile changes to the letters of "E" as the incident light with the angle of -40° is blocked (left image in Figure 6D). The complete vortex array appears when two light beams strike the sample simultaneously, as illustrated in right image in Figure 6D. The measured light intensity images agree well with the theoretical results. The measured broadband effect of this designed metasurface is depicted in Figure S5 (Supplementary Information). The flexible angle control of the angle-multiplexed metasurface enables us to recombine the form of vortex array at will. Such a method can improve information diversification and safety to a certain extent. In addition, we can employ polarization as another degree of freedom to modulate the generated vortex array to further increase the multiplexing capacity and safety.

CONCLUSION

In summary, we demonstrate the manipulation of angular-multiplexed multichannel vortex arrays based on ultra-thin geometric metasurfaces. Under the illumination of circularly polarized light, the metasurface emits various vortex arrays with different diffraction angles. And the topological charge of vortex array is spatially variant. Furthermore, the diffraction angle of the reconstructed multichannel vortex arrays can be adjusted by changing the illumination angle of the incident light. Capitalizing on this advantage, a metasurface that can recombine a new vortex array is realized. The experimental results agree well with the theoretical results. Our approach provides an effective way to increase the information capacity and safety and offers a new avenue for many applications such as optical communication, optical display, and optical trapping.

Limitations of the study

Restricted by the limited measuring space and the microscopic detection system is fixed, we cannot detect all multichannel vortex arrays at the same plane. The diffracted multichannel vortex arrays are separately detected by changing the illumination angle.

METHODS

All methods can be found in the accompanying [Transparent Methods supplemental file](#).

SUPPLEMENTAL INFORMATION

Supplemental Information can be found online at <https://doi.org/10.1016/j.isci.2021.102107>.

ACKNOWLEDGMENTS

This work was supported by the National Natural Science Funds of China under Grant Nos. 61822511, 61705234 and the Youth Innovation Promotion Association of the Chinese Academy of Sciences.

AUTHORS CONTRIBUTION

J.J. conceived the idea and performed the experimental measurements. X.L., M.P., Y.G., and Z.Z., performed the theoretical calculations, numerical simulations, and data analysis. P.G. fabricated the sample. X.G.L. supervised the whole project. J.J. wrote the manuscript, and all the authors reviewed the manuscript.

DECLARATION OF INTERESTS

The authors declare there is no competing interests.

Received: November 13, 2020

Revised: December 21, 2020

Accepted: January 20, 2021

Published: February 19, 2021

REFERENCES

- Aieta, F., Genevet, P., Kats, M.A., Yu, N., Blanchard, R., Gaburro, Z., and Capasso, F. (2012). Aberration-free ultrathin flat lenses and axicons at telecom wavelengths based on plasmonic metasurfaces. *Nano Lett.* *12*, 4932–4936.
- Allen, L., Beijersbergen, M.W., Spreeuw, R., and Woerdman, J. (1992). Orbital angular momentum of light and the transformation of Laguerre-Gaussian laser modes. *Phys. Rev. A* *45*, 8185.
- Chen, S., Liu, W., Li, Z., Cheng, H., and Tian, J. (2020). Metasurface-empowered optical multiplexing and multifunction. *Adv. Mater.* *32*, 1805912.
- Dholakia, K., Reece, P., and Gu, M. (2008). Optical micromanipulation. *Chem. Soc. Rev.* *37*, 42–55.
- Gibson, G., Courtial, J., Padgett, M., Vasnetsov, M., Pas'ko, V., Barnett, S., and Franke-Arnold, S. (2004). Free-space information transfer using light beams carrying orbital angular momentum. *Opt. Express* *12*, 5448–5456.
- Guo, J., Wang, T., Quan, B., Zhao, H., Gu, C., Li, J., Wang, X., Situ, G., and Zhang, Y. (2019). Polarization multiplexing for double images display. *Opto-electron. Adv.* *2*, 180029.
- Huang, L., Chen, X., Mühlenbernd, H., Li, G., Bai, B., Tan, Q., Jin, G., Zentgraf, T., and Zhang, S. (2012). Dispersionless phase discontinuities for controlling light propagation. *Nano Lett.* *12*, 5750–5755.
- Huang, L., Chen, X., Mühlenbernd, H., Zhang, H., Chen, S., Bai, B., Tan, Q., Jin, G., Cheah, K.-W., and Qiu, C.-W. (2013). Three-dimensional optical holography using a plasmonic metasurface. *Nat. Commun.* *4*, 2808.
- Huang, L., Song, X., Reineke, B., Li, T., Li, X., Liu, J., Zhang, S., Wang, Y., and Zentgraf, T. (2017). Volumetric generation of optical vortices with metasurfaces. *ACS Photon.* *4*, 338–346.
- Jiang, Z.H., Kang, L., Hong, W., and Werner, D.H. (2018). Highly efficient broadband multiplexed millimeter-wave vortices from metasurface-enabled transmit-arrays of subwavelength thickness. *Phys. Rev. Appl.* *9*, 064009.
- Jin, J., Li, X., Pu, M., Ma, X., and Luo, X. (2018). Wavelength-dependent three-dimensional volumetric optical vortices modulation based on metasurface. *IEEE Photo. J.* *10*, 1–8.
- Jin, J., Pu, M., Wang, Y., Li, X., Ma, X., Luo, J., Zhao, Z., Gao, P., and Luo, X. (2017). multi-channel vortex beam generation by simultaneous amplitude and phase modulation with two-dimensional metamaterial. *Adv. Mater. Technol.* *2*, 1600201.
- Khonina, S., Kotlyar, V., Soifer, V., Pääkkönen, P., Simonen, J., and Turunen, J. (2001). An analysis of the angular momentum of a light field in terms of angular harmonics. *J. Mod. Opt.* *48*, 1543–1557.
- Lavery, M.P., Speirits, F.C., Barnett, S.M., and Padgett, M.J. (2013). Detection of a spinning object using light's orbital angular momentum. *Science* *341*, 537–540.
- Lei, T., Zhang, M., Li, Y., Jia, P., Liu, G.N., Xu, X., Li, Z., Min, C., Lin, J., and Yu, C. (2015). Massive individual orbital angular momentum channels for multiplexing enabled by Dammann gratings. *Light Sci. Appl.* *4*, e257.
- Li, X., Chen, L., Li, Y., Zhang, X., Pu, M., Zhao, Z., Ma, X., Wang, Y., Hong, M., and Luo, X. (2016). Multicolor 3D meta-holography by broadband plasmonic modulation. *Sci. Adv.* *2*, e1601102.
- Li, Z., Palacios, E., Butun, S., and Aydin, K. (2015). Visible-frequency metasurfaces for broadband anomalous reflection and high-efficiency spectrum splitting. *Nano Lett.* *15*, 1615–1621.
- Lin, J., Mueller, J.B., Wang, Q., Yuan, G., Antoniou, N., Yuan, X.-C., and Capasso, F. (2013). Polarization-controlled tunable directional coupling of surface plasmon polaritons. *Science* *340*, 331–334.
- Liu, J., Min, C., Lei, T., Du, L., Yuan, Y., Wei, S., Wang, Y., and Yuan, X.-C. (2016). Generation and detection of broadband multi-channel orbital angular momentum by micrometer-scale meta-reflectarray. *Opt. Express* *24*, 212–218.
- Ma, X., Pu, M., Li, X., Guo, Y., and Luo, X. (2019). All-metallic wide-angle metasurfaces for multifunctional polarization manipulation. *Opto-electron. Adv.* *2*, 180023.
- Ni, X., Ishii, S., Kildishev, A.V., and Shalaev, V.M. (2013a). Ultra-thin, planar, Babinet-inverted plasmonic metalenses. *Light Sci. Appl.* *2*, e72.
- Ni, X., Kildishev, A.V., and Shalaev, V.M. (2013b). Metasurface holograms for visible light. *Nat. Commun.* *4*, 2807.
- Pu, M., Li, X., Ma, X., Wang, Y., Zhao, Z., Wang, C., Hu, C., Gao, P., Huang, C., Ren, H., et al. (2015a). Catenary optics for achromatic generation of perfect optical angular momentum. *Sci. Adv.* *1*, e1500396.
- Pu, M., Zhao, Z., Wang, Y., Li, X., Ma, X., Hu, C., Wang, C., Huang, C., and Luo, X. (2015b). Spatially and spectrally engineered spin-orbit interaction for achromatic virtual shaping. *Sci. Rep.* *5*, 9822.
- Ren, H., Briere, G., Fang, X., Ni, P., Sawant, R., Heron, S., Chenot, S., Veizan, S., Damilano, B., and Brandli, V. (2019). Metasurface orbital angular momentum holography. *Nat. Commun.* *10*, 2986.
- Ren, H., Li, X., Zhang, Q., and Gu, M. (2016). On-chip noninterference angular momentum multiplexing of broadband light. *Science* *352*, 805–809.
- Tamburini, F., Anzolin, G., Umbriaco, G., Bianchini, A., and Barbieri, C. (2006). Overcoming

the Rayleigh criterion limit with optical vortices. *Phys. Rev. Lett.* **97**, 163903.

Wen, D., Chen, S., Yue, F., Chan, K., Chen, M., Ardron, M., Li, K.F., Wong, P.W.H., Cheah, K.W., Pun, E.Y.B., et al. (2016). Metasurface device with helicity-dependent functionality. *Adv. Opt. Mater.* **4**, 321–327.

Yu, N., and Capasso, F. (2014). Flat optics with designer metasurfaces. *Nat. Mater.* **13**, 139–150.

Yu, N., Genevet, P., Kats, M.A., Aieta, F., Tetienne, J.-P., Capasso, F., and Gaburro, Z.

(2011). Light propagation with phase discontinuities: generalized laws of reflection and refraction. *Science* **334**, 333–337.

Zhang, F., Pu, M., Gao, P., Jin, J., Li, X., Guo, Y., Ma, X., Luo, J., Yu, H., and Luo, X. (2020a). Simultaneous full-color printing and holography enabled by centimeter-scale plasmonic metasurfaces. *Adv. Sci.* **7**, 1903156.

Zhang, S., Huo, P., Zhu, W., Zhang, C., Chen, P., Liu, M., Chen, L., Lezec, H.J., Agrawal, A., Lu, Y., et al. (2020b). Broadband detection of multiple

spin and orbital angular momenta via dielectric metasurface. *Laser Photon. Rev.* **14**, 2000062.

Zhang, X., Jin, J., Pu, M., Li, X., Ma, X., Gao, P., Zhao, Z., Wang, Y., Wang, C., and Luo, X. (2017). Ultrahigh-capacity dynamic holographic displays via anisotropic nanoholes. *Nanoscale* **9**, 1409–1415.

Zheng, G.X., Muhlenbernd, H., Kenney, M., Li, G.X., Zentgraf, T., and Zhang, S. (2015). Metasurface holograms reaching 80% efficiency. *Nat. Nanotechnol.* **10**, 308–312.

iScience, Volume 24

Supplemental Information

Angular-multiplexed multichannel optical vortex arrays generators based on geometric metasurface

Jinjin Jin, Xiong Li, Mingbo Pu, Yinghui Guo, Ping Gao, Mingfeng Xu, Zuojun Zhang, and Xiangang Luo

Supplemental Figures

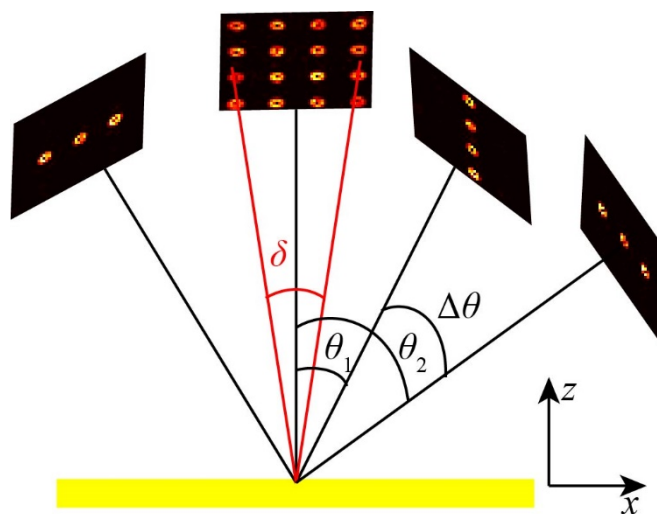


Figure S1. Schematic of diffraction effect of multichannel vortex arrays. θ_i ($i = 1, 2, 3 \dots$) is the diffraction angle, $\Delta\theta$ is the absolute value of diffraction angle difference for two adjacent vortex arrays and δ is the field angle of the single vortex array. Related to Transparent Methods (Section S1. Diffraction properties of the multichannel vortex arrays).

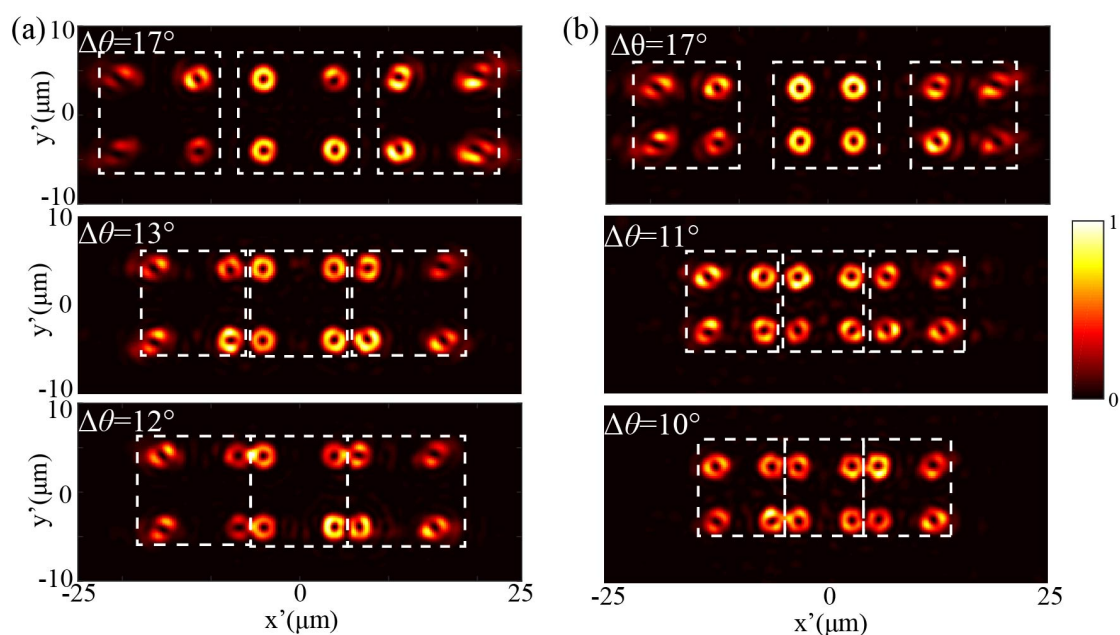


Figure S2. The diffraction effect of the vortex arrays with different diffraction angles and field angles at wavelength of 632.8 nm. (a) The diffraction effect of the first generator. The vortex arrays in the three white dashed boxes represent three vortex arrays. For the top image, the diffraction angles of the three vortex arrays are -17° , 0° and 17° , respectively. For the middle image, the diffraction angles of the three vortex arrays are -13° , 0° and 13° , respectively. For the bottom image, the diffraction angles of the three vortex arrays are -12° , 0° and 12° , respectively. The field angle of each

vortex array is about 12.5° . (b) The diffraction effect of second generator. The vortex arrays in the three white dashed boxes represent three vortex arrays. For the top image, the diffraction angles of the three vortex arrays are -17° , 0° and 17° , respectively. For the middle image, the diffraction angles of the three vortex arrays are -11° , 0° and 11° , respectively. For the bottom image, the diffraction angles of the three vortex arrays are -10° , 0° and 10° , respectively. The field angle of each vortex array is about 10.5° . Related to Transparent Methods (Section S1. Diffraction properties of the multichannel vortex arrays).

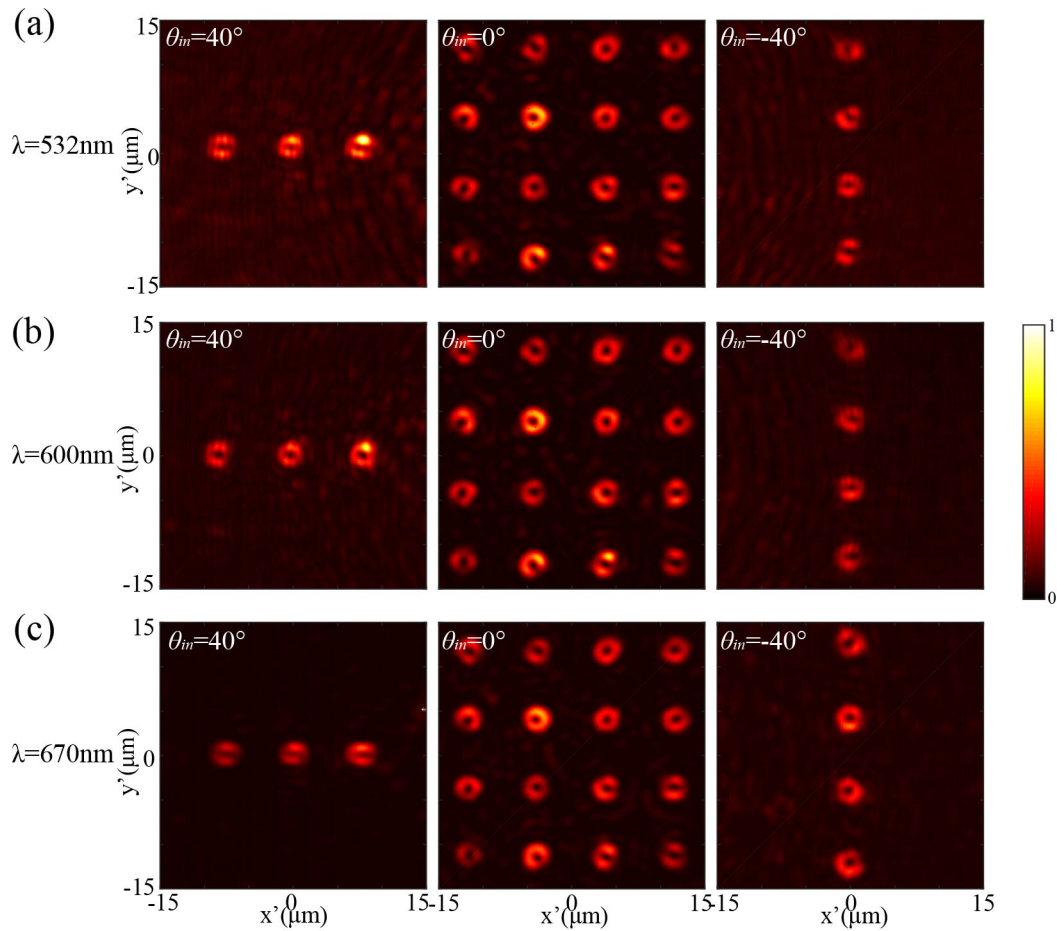


Figure S3. Schematic of the broadband effect of first multichannel vortex arrays generator (a) The measured vortex arrays intensity profiles at wavelength of 532 nm; (b) The measured vortex arrays intensity profiles at wavelength of 600 nm; (c) The measured vortex arrays intensity profiles at wavelength of 670 nm; The incident angle of the left, middle and right figures is 40° , 0° and 40° , respectively. Related to Figure 5 and Transparent Methods (Section S2. Broadband properties of designed metasurfaces).

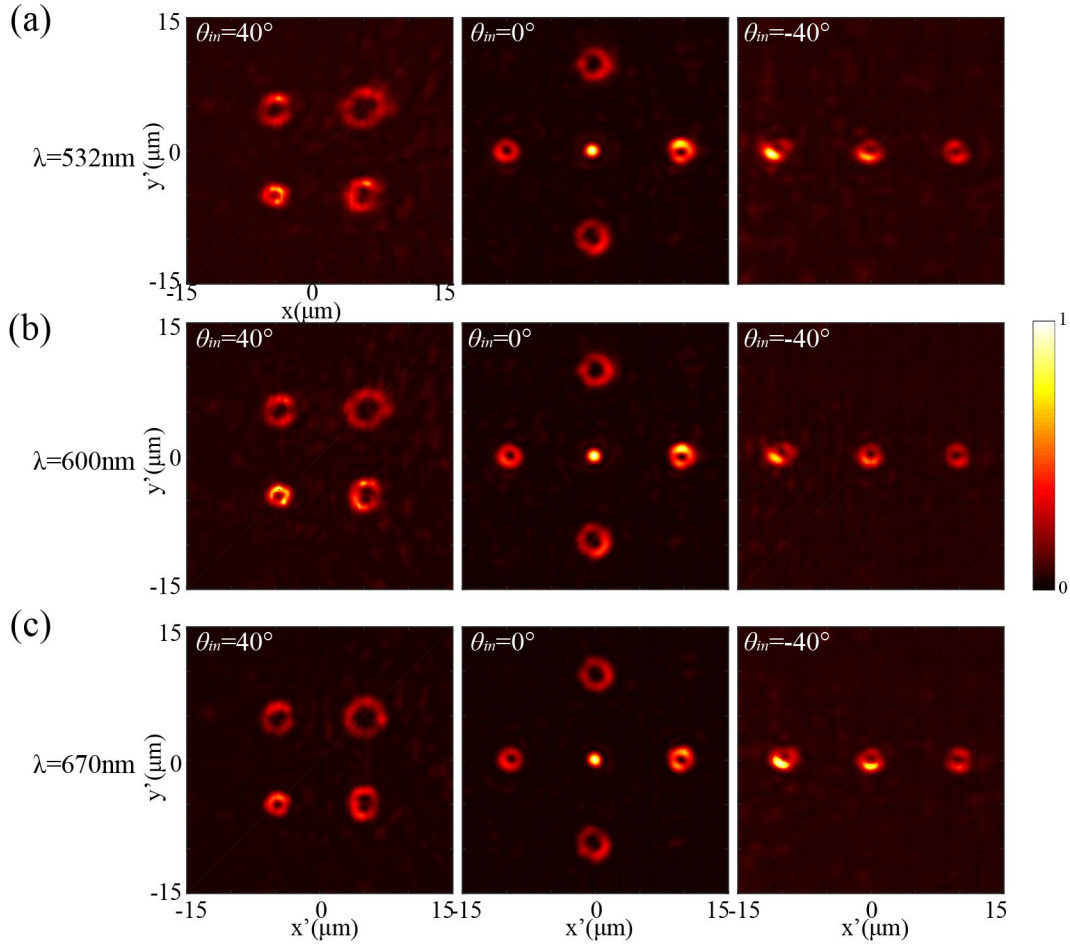


Figure S4. Schematic of broadband effect of second multichannel vortex arrays generator. (a) The measured vortex arrays intensity profiles at wavelength of 532 nm; (b) The measured vortex arrays intensity profiles at wavelength of 600 nm; (c) The measured vortex arrays intensity profiles at wavelength of 670 nm; The incident angle of the left, middle and right figures is 40° , 0° and 40° , respectively. Related to Figure 5 and Transparent Methods (Section S2. Broadband properties of designed metasurfaces).

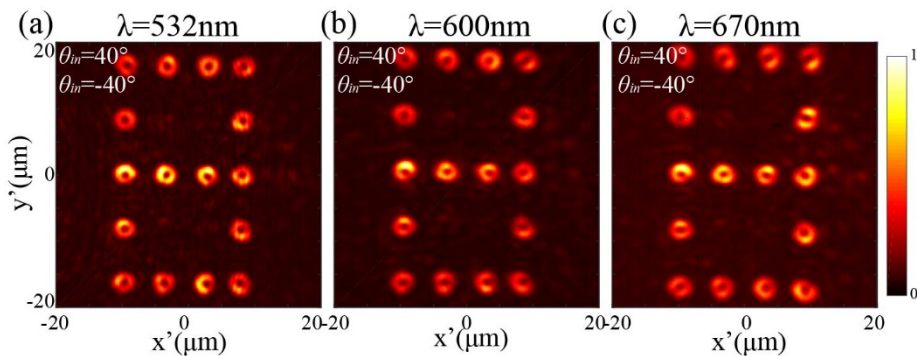


Figure S5. Schematic of the broadband effect of third metasurface. (a) The measured recombined complete vortex array intensity profile at wavelength of 532 nm; (b) The measured recombined complete vortex array intensity profile at wavelength of 600 nm; (c) The measured recombined complete vortex array intensity profile at wavelength of 670 nm. Related to Figure 6 and Transparent Methods (Section S2. Broadband

properties of designed metasurfaces).

Transparent Methods

Section S1. Diffraction properties of the multichannel vortex arrays.

In the design process, the diffraction angle and the size of vortex array are two important parameters, which determined the existence of light crosstalk and the final number of vortex arrays. The multichannel vortex arrays generator can scatter numerous vortex arrays without crosstalk between them by elaborately choosing the two parameters. Here, the $\Delta\theta$ defined by the absolute value of diffraction angle difference for two adjacent vortex arrays and the field angle of δ which represents the size of a single vortex array (Figure S1) are applied to analyze the diffraction properties of multichannel generators. Assuming that there are two multichannel vortex arrays generators, as shown in Figure S2. For the first generator, the field angle δ of each vortex array is about 12.5° , the diffraction effects of the vortex arrays with the change of absolute value of diffraction angle difference is illustrated in Figure S2(a). When the absolute value of diffraction angle difference is set as $\Delta\theta = 17^\circ$ (top image in Figure S2(a)) and $\Delta\theta = 13^\circ$ (middle image in Figure S2(a)), respectively, there is no crosstalk between the vortex arrays. The interference appeared as the absolute value of diffraction angle difference is set as $\Delta\theta = 12^\circ$ (bottom image in Figure S2(a)). Therefore, the minimum absolute value of diffraction angle difference for the first generator is approximately 13° . For the second generator, the field angle δ of each vortex array is about 12.5° . The interference appeared when the absolute value of diffraction angle difference is set as $\Delta\theta = 10^\circ$ (bottom image in Figure S2(b)). The proper minimum absolute value of diffraction angle difference for the second generator is about 11° (middle image in Figure S2(b)). Based on the above results we can draw a conclusion that as long as the maximum field angle δ is less than the minimum absolute value of diffraction angle difference $\Delta\theta$, there will be no crosstalk between the vortex arrays. And the maximum number of vortex arrays can also be further confirmed by the ratio of angle range of free space to the minimum absolute value of diffraction angle difference. Considering the finite angle range of free space at the transmission side, which ranging from -90° to 90° , the maximum number of vortex arrays generated by the two assuming generators can be 13 and 16, respectively. It worth mentioning that the maximum number of vortex arrays can be further improved by reducing the field angle of the vortex array.

Section S2. Broadband properties of designed metasurfaces.

The phase shift of the designed metasurface is only determined by the orientation of the elliptical nanoholes and the helicity of the incident light, which means that the fabricated generators can work at broadband. The broadband effect of the designed generator is verified by measuring the reconstruction intensity profiles at different wavelengths from 532 nm to 670 nm, as shown in Figures S3, S4 and S5. The wavelengths of the incident light are set as 532 nm, 600 nm and 670 nm, respectively.